ISSN 1063-7745, Crystallography Reports, 2023, Vol. 68, No. 2, pp. 210–217. © Pleiades Publishing, Inc., 2023.
Russian Text © The Author(s), 2023, published in Kristallografiya, 2023, Vol. 68, No. 2, pp. 196–203.

DIFFRACTION AND SCATTERING OF IONIZING RADIATIONS

Computer Simulation of the Effect of Coherent Dynamical Diffraction of Synchrotron Radiation in Crystals of Arbitrary Shape and Structure

V. G. Kohn[a,b,*]

[a] *National Research Centre "Kurchatov Institute," Moscow, 123182 Russia*
[b] *Shubnikov Institute of Crystallography, Federal Scientific Research Centre "Crystallography and Photonics," Russian Academy of Sciences, Moscow, 119333 Russia*
**e-mail: kohnvict@yandex.ru*

Received December 14, 2022; revised December 23, 2022; accepted December 23, 2022

Abstract—A new scheme for the numerical solution of Takagi–Taupin equations, which makes it possible to simulate the effect of synchrotron radiation diffraction in crystals of arbitrary structure, is described in detail. The new scheme is convenient to perform calculations for crystals of arbitrary shape. The rectangular coordinate system and the algorithm for calculating derivatives at half of step have proven their efficiency and are used, but the recurrence equations of this algorithm have been modified towards simplification. The boundary conditions are in no way related to the crystal boundaries. A computer program is developed, and two examples are considered for the cases of diffraction in the Laue and Bragg geometries, for which the analytical solutions are known. The calculation results are in complete agreement with these solutions.

DOI: 10.1134/S1063774523020086

INTRODUCTION

The effect of X-ray diffraction in crystals was revealed experimentally soon after discovering X rays; i.e., at the beginning of the XX century. As is well known [1, 2], the experimental results obtained at that time were inconsistent with the predictions of the first diffraction theory, developed by Darwin, and then with the predictions of the more general Ewald theory, elaborated by Laue to the modern form. The theory was developed for large perfect crystals, while the crystals were imperfect in that time. Specifically, they were polycrystals, in which small-size regions having a perfect structure, and the samples studied consisted of many such domains with different orientations. In addition, the radiation was incoherent, as a result of which different parts of a sample diffracted radiation independently.

The X-ray diffraction under these conditions was referred to as kinematic, and calculations were performed on the assumption that the diffracted wave has a low intensity and does not affect the incident wave. The Ewald–Laue theory takes into account this influence; and this continuation leads to a number of interesting features of the effect itself. The X-ray diffraction under conditions of mutual influence of transmitted and diffracted waves was called dynamic. Nevertheless, even the kinematic theory of X-ray diffraction has played a very important role in the development of crystallography and continues to be highly demanded [3].

The problem with coherence was solved in 1959 [4] in the scheme of experiment in transmission (Laue geometry), using a narrow slit transmitting an X-ray beam with a transverse size of no more than 10 μm. Under these conditions radiation penetrates a thick crystal within a Borrmann fan. Extinction bands were observed at the center of this fan; i.e., the coherent effect of interference of waves with different refractive indices was observed. However, to describe this experiment, it was necessary to modify the theory developed initially for incident plane waves.

This was done for the first time by Kato [5] in 1961; he used the Fourier transform of the X-ray wave function. In the next year Takagi [6] proposed a more universal modification of the theory in the form of a system of differential equations, which are simpler than the initial Maxwell equations but take into account in full measure the dynamic effects characteristic of the X-ray diffraction in single crystals. However, no solution to these equations was presented. In 1964 Taupin proposed the same equations, and then applied them for the first time for numerical calculation of the X-ray diffraction in a crystal with a dislocation [7]. As a result, the abbreviation TTE (Takagi–Taupen equations) was assigned to these equations.

Many publications appeared in the next years, which reported results of numerical calculations of images of single crystals in the form of a plate, containing single structure defects, such as dislocations, stacking faults, etc., as well as a plate subjected to external impacts, for example, bending or point pressure on the plate surface. Methods of numerical solution of TTE were applied. Discussion of the results of these studies, as well as the corresponding references, can be found in reviews [8–10].

It was also shown that the solution to TTE for a perfect crystal with arbitrary boundary conditions can be presented in the form of integrals over the crystal boundary of the product of the X-ray wave function at the boundary and the so-called influence function, which is the solution to TTE for a point source on the boundary [1, 2]. Influence functions were obtained for the Laue geometry with an arbitrary crystal boundary and the Bragg geometry for a crystal in the form of a plate of finite thickness. A typical example of using these solutions was published in [11, 12]. References to the preceding publications can also be found there.

Concerning the methods of numerical solution of TTE, the method denoted as HSD (half-step derivative) in [13] was most thoroughly developed. It uses the rectangular coordinate system with a boundary on the crystal surface and different steps over axes along the surface and perpendicular to it. In the Laue geometry the X-ray wave function is calculated from the input surface of crystal plate (X axis) to the output surface on the lines parallel to the plate surface; i.e., a solution for a plate whose thickness contains an integer number of steps over the normal to the surface (Z axis) at each step. Only lattice strains were generally investigated.

In the case of Bragg geometry the boundary conditions were considered both on the input surface and on the lateral crystal surface on a line along the incident beam direction. Two opposite schemes were used in the calculations, specifically, a convergent scheme for the incident plane waves and a divergent scheme for a source on the surface. In the first scheme the input (incident) beam was coherent on a large but finite fragment of the X axis, while the result was obtained on a smaller interval, because at each step along the Z axis the interval along the X axis decreased by one step.

However, for many years it was impossible to obtain a coherent wave with a wide front under laboratory conditions. For this reason narrow beams at the input were considered, which illuminated a crystal within a Borrmann fan. In this scheme, at each step along the Z axis the interval along the X axis increased by one step, and initially the X-ray wave function differed from zero at few points on the X axis. At other points the function was zero; i.e., was also known. The development of synchrotron radiation sources extended the possibilities of studying the diffraction effect in crystals. It became possible to study crystals of relatively small sizes and arbitrary shape [14]. On the other hand, publications appeared in which other methods for solving TTE were developed (see, e.g., [15, 16] and references therein).

However, it was noted in 1971 [17] that it is reasonable to select three regions in a crystal, which can be considered separately: the region of perfect crystal, the region of deformed crystal, and the region in which diffraction is completely absent. It is natural to develop this concept and supplement the crystal model with regions that may contain a material with another density and even voids, as occurs in silicon carbide crystals [18] or crystals of complex shape [19, 20].

In this paper we propose and describe in detail a new method of numerical solution of TTE, which can be applied to crystals of arbitrary shape and structure. The rectangular coordinate system and the HSD algorithm [13] proved their efficiency and are used, but the recurrence formulae of this method are modified. A new feature is that the boundary conditions are set on the X axis, which is in no way related to the crystal shape. The solution is obtained successively when moving along the Z axis, which is parallel to the reflecting atomic planes of the crystal.

The space in which TTE are solved may contain both regions with a lattice and non-diffraction regions with different density and structure, including voids. Diffraction occurs only at a very small deviation of interplanar spacing or orientation of planes from the state in which the Bragg condition is satisfied. A computer program implementing the proposed method has been developed. Two cases of diffraction in a rectangular crystal, in which one face of a smaller size (end face) is parallel to the X axis and the lateral faces are parallel to the Z axis, were considered as application examples. In the first case a narrow incident beam enters a crystal from the end face. The Laue geometry is implemented initially, and then the crystal lateral faces change the diffraction conditions. In the second case a wide beam is incident on a plate lateral face; this situation corresponds to the Bragg geometry. More complex problems will be considered elsewhere.

METHOD OF NUMERICAL SOLUTION OF TTE

Let us define half-space as a set of all coordinates x and only positive coordinates z of the rectangular coordinate system, as shown in Fig. 1. In the two-wave case of diffraction the result is independent of the y coordinate if the medium is homogeneous in this direction. Otherwise, the dependence on this coordinate has a parametric character and is trivially taken into account. This half-space contains regions of arbitrary shape with a lattice containing atomic planes oriented parallel to the Z axis, with a certain interplanar spacing. These planes can be presented by the reciprocal lattice vector $\mathbf{h}$ lying in the (XZ) plane.

The slowly varying complex amplitudes for the plane waves with the wave vectors $\mathbf{k}_0$ and $\mathbf{k}_h = \mathbf{k}_0 + \mathbf{h}$ are known on the X axis at $z = 0$. The parameter $\alpha = (k_h^2/k_0^2 - 1)$ has a very small value, comparable with the real part of the complex diffraction parameters χ_0, χ_h, and χ_{-h}, which are equal to the coefficients of the Fourier series for the periodic polarizability of the medium on reciprocal lattice vectors $\mathbf{0}$, $\mathbf{h}$, $-\mathbf{h}$. Along with the regions having the aforementioned lattice, the half-space may also contain regions with other parameters; i.e., in the general case, the parameters χ_0, χ_h, and χ_{-h} are coordinate-dependent.

The coordinate dependence is determined by not only the lattice strain but also other changes in both the structure and electron density. In particular, the parameters χ_h and χ_{-h} (in amorphous regions) or all parameters (in the regions where material is absent) can be zero. Strains are described by the displacement vector $\mathbf{u}$ of atoms from the ideally periodic state. As a result of the atomic displacements the parameter χ_h is multiplied by a factor $\exp(-i\mathbf{hu})$ and the parameter χ_{-h} is multiplied by a complex conjugate factor. These factors are also coordinate-dependent. In the general case not only phase but also the modulus of complex parameters may change.

Hence, it is reasonable to write the initial TTE in a simpler form than in [20], without indicating the specific type of the coordinate dependence, specifically,

$$\begin{aligned} \frac{p}{2}\frac{\partial E_0}{\partial s_0} &= X_0 E_0 + X_{-h} E_h, \\ \frac{p}{2}\frac{\partial E_h}{\partial s_h} &= [X_0 - A]E_h + X_h E_0, \end{aligned} \tag{1}$$

where X_0, X_h, X_{-h}, and A are new complex parameters, which are obtained after multiplying the parameters χ_0, χ_h, χ_{-h}, and α by the factor $iKp/4$. Hereinafter, $K = 2\pi/\lambda$ (λ is the X-ray wavelength). The derivatives in (1) are written with respect to coordinates, which are counted over directions of the vectors $\mathbf{k}_0$ and $\mathbf{k}_h$, as shown in Fig. 1. The parameter p in these equations cancels out and does not affect the result. It acquires sense only when the algorithm of approximate calculation of derivatives is used.

Calculations are performed on an oblique coordinate system of computational grid points, shown in Fig. 1. The key parameter is the step along the Z axis. It is chosen by the user as $d_z = d$. The step along the X axis cannot be arbitrary; it is $d_x = 2d \tan\theta_B$, where θ_B is the Bragg angle, equal to half of the angle between the vectors $\mathbf{k}_0$ and $\mathbf{k}_h$. At each step along the Z axis the grid points along the X axis are displaced by half step. The values of the functions are set and determined at the points of intersection of lines along the wave vector directions. At each step along the Z axis all values on the X axis of the previous row are known.

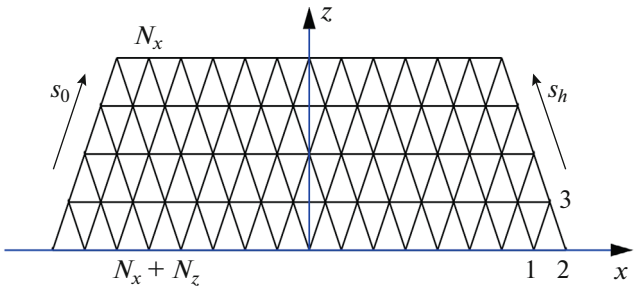

Fig. 1. Rectangular coordinate system and grid of points for numerical solution of TTE within the convergence scheme. The wave function is set on $(N_x + N_z)$ segments along the X axis at the input ($z = 0$). At the output, after N_z steps along the Z axis, the answer is obtained on N_x segments.

At the very beginning they are known from the boundary conditions.

Let us consider three grid points with numbers 1, 2, and 3 in the right bottom corner of Fig. 1. At each step of Eq. (1) a relationship is installed between the known fields $\mathbf{E}^{(\text{old})} = (E_0^{(1)}, E_h^{(1)}, E_0^{(2)}, E_h^{(2)})$ at points 1 and 2 and the unknown fields $\mathbf{E}^{(\text{new})} = (E_0^{(3)}, E_h^{(3)})$ at point 3. Both Eqs. (1) are written for points in the middle of segments between the pair of points 1 and 3 and the pair of points 2 and 3. The derivative is replaced with the ratio of the difference in fields in each pair of points to the distance between points, which is equal to $p = d/\cos\theta_B$, and the values of functions on the right-hand side of the equations is replaced by the half-sum of values at the same points.

After these replacements Eqs. (1) can approximately be written as

$$\begin{aligned} E_0^{(3)} - E_0^{(1)} &= X_0^{(1)} E_0^{(1)} + X_{-h}^{(1)} E_h^{(1)} \\ &+ X_0^{(3)} E_0^{(3)} + X_{-h}^{(3)} E_h^{(3)}, \\ E_h^{(3)} - E_h^{(2)} &= X_h^{(2)} E_0^{(2)} + X_1^{(2)} E_h^{(2)} \\ &+ X_h^{(3)} E_0^{(3)} + X_1^{(3)} E_h^{(3)}. \end{aligned} \tag{2}$$

Hereinafter, $X_1 = X_0 - A$. The superscripts indicate the point at which the values of functions must be taken. Equation (2) implicitly determines the unknown values in terms of the known ones. It is convenient to write the solution to this system of equations in the matrix form: $\mathbf{E}^{(\text{new})} = \mathbf{M}_{2,4} \times \mathbf{E}^{(\text{old})}$. The matrix can be written as

$$\mathbf{M}_{2,4} = \frac{1}{D}\begin{pmatrix} X_{0+}^{(1)} X_{1-}^{(3)}, & X_{-h}^{(1)} X_{1-}^{(3)}, & X_h^{(2)} X_{-h}^{(3)}, & X_{1+}^{(2)} X_{-h}^{(3)} \\ X_{0+}^{(1)} X_h^{(3)}, & X_{-h}^{(1)} X_h^{(3)}, & X_h^{(2)} X_{0-}^{(3)}, & X_{1+}^{(2)} X_{0-}^{(3)} \end{pmatrix}, \tag{3}$$

where

$$\begin{aligned} D = X_{0-}^{(3)} X_{1-}^{(3)} - X_h^{(3)} X_{-h}^{(3)}, \quad X_{0\pm} = 1 \pm X_0, \\ X_{1\pm} = 1 \pm X_1, \end{aligned} \tag{4}$$

Inside a homogeneous or slowly varying medium the change in the diffraction parameters at all three points can be neglected, as was done in the previous studies. However, the differences can be rather large at the interface between media, especially on the crystal boundary. Note that the matrix has a certain symmetry. Some factors are repeated both over vertical and over horizontal.

Numerical solution of the problem is reduced to successive consideration of all triangles along the X axis. Starting with the first line, where boundary conditions are set at $N_x + N_z + 1$ points, we obtain the next line with a number of points smaller by unity. After N_z steps the number of points with a known solution is $N_x + 1$. It is reasonable to write the answer in a rectangle with the numbers of points $(N_x + 1)$ along the X axis and $(N_z + 1)$ along the Z axis with omitted odd numbers of points, whereas the number N_x and N_z must be taken even. This convergence scheme suggests that the values of the wave function beyond the considered segment are unknown at $z = 0$. Therefore, a reliable answer cannot be obtained at $z = dN_z$ beyond the interval of width d_xN_x.

The divergence scheme assumes as known that, at $z = 0$, the wave function is zero beyond the considered segment. For this reason the calculation is performed exactly in the same way, but with addition of one point with zero values on the left and one point with zero values on the right at each step along the Z axis on the X axis. Thus, the number of initial points increases by two, and the number of final points increases by one. Correspondingly, the interval of width d_xN_x at $z = 0$ turns into the interval $d_x(N_x + N_z)$ at $z = dN_z$. If a calculation in this version is performed within the convergence scheme, one must add $2N_z$ zeros to the input data and perform further calculation with the same result.

The calculation for an amorphous medium can be performed according to the same scheme as for a crystal, only with zero values of the parameters X_h, X_{-h}, and A. In this case the matrix takes a very simple form: only the first element in the first row and the last element in the second row of this matrix are nonzero. However, in this case the solution can be obtained more easily directly from Eq. (2) in the form

$$E_0^{(3)} = (X_{0+}^{(1)}/X_{0-}^{(3)})E_0^{(1)}, \quad E_h^{(3)} = (X_{0+}^{(2)}/X_{0-}^{(3)})E_h^{(2)}. \quad (5)$$

The corresponding relations for a void are the same with the only difference: the parameters $X_{0\pm}$ are equal to unity. The calculation for these regions can be performed much more rapidly than for the crystal. Note that a matrix for these regions was reported in [20], but multiplication of a complex matrix by a complex vector at many points increases the calculation time and is unreasonable.

The most general way to set the shape of a crystal, as well as that of an amorphous region, is as follows. The limits $x_1(z)$ and $x_2(z)$, between which a crystal or an amorphous region is located on the X axis, are determined at each z value. If the limits coincide for some coordinate z, the region is absent for such coordinates. In this way one can determine any set of crystals of arbitrary shape. Moreover, this approach shortens the program operation time due to the simpler way of determining the medium for calculating the transition matrix. If the medium does not change, it is not necessary to recalculate the matrix.

RESULTS AND DISCUSSION

The computer program for numerical simulation of diffraction in crystals of arbitrary shape was developed within the more general program XRWP1 [21], designed to solve all (when possible) problems of coherent X-ray optics, and constitutes its part. The description of the program operation can be found on the aforementioned website. In this section two examples of its application for calculating the diffraction in a rectangular crystal are considered. The relatively simple crystal shape makes it possible to compare the calculated dependences with the previous solutions obtained in a different way. However, this method gives more information even during calculation, showing a detailed distribution of radiation intensity throughout the entire volume.

In both cases a silicon crystal and the 220 reflection are considered; the photon energy is $E = 10$ keV and the Bragg angle is $\theta_B = 18.84°$. The radiation incident on the crystal is a plane wave limited by a slit of size S in the direction perpendicular to the vector $\mathbf{k}_0$. The step d of the grid of points along the Z axis was taken to be 0.04 μm for numerical calculations. The diffraction parameters were obtained using the on-line-program [22]. The crystal faces are parallel to the X (width) and Z (length) axes.

First case. A crystal has sizes $W_c = 50$ μm in width and $L_c = 120$ μm in length. The incident beam is fairly narrow ($S = 0.4$ μm), and its center is located at the point $x = 0$. Under these conditions, the width of the Borrmann fan base is $W_B = 2L\tan(\theta_B) = 82$ μm; i.e., it exceeds the crystal width. The crystal is in the exact Bragg position; i.e., the angular deviation $\Delta\theta = 0$. Note that the parameter $\alpha = -2\sin(2\theta_B)\Delta\theta$. The divergence scheme was used in the calculation. The calculation results are presented in Fig. 2. Since the diffracted radiation has a very low intensity for a narrow beam at the input, it is convenient to show the contrast on the logarithmic scale.

Figure 2 shows the distribution of the natural logarithm of relative intensity for the transmitted beam $(\ln(I_T/I_0))$ on the left and the corresponding distribution for the reflected beam $(\ln(I_R/I_0))$ on the right. On the input surface, $I_T = I_0$ inside the slit. To obtain the maximum contrast, the color scale shows the interval from the minimum value I_{mi}/I_0 to the maximum value

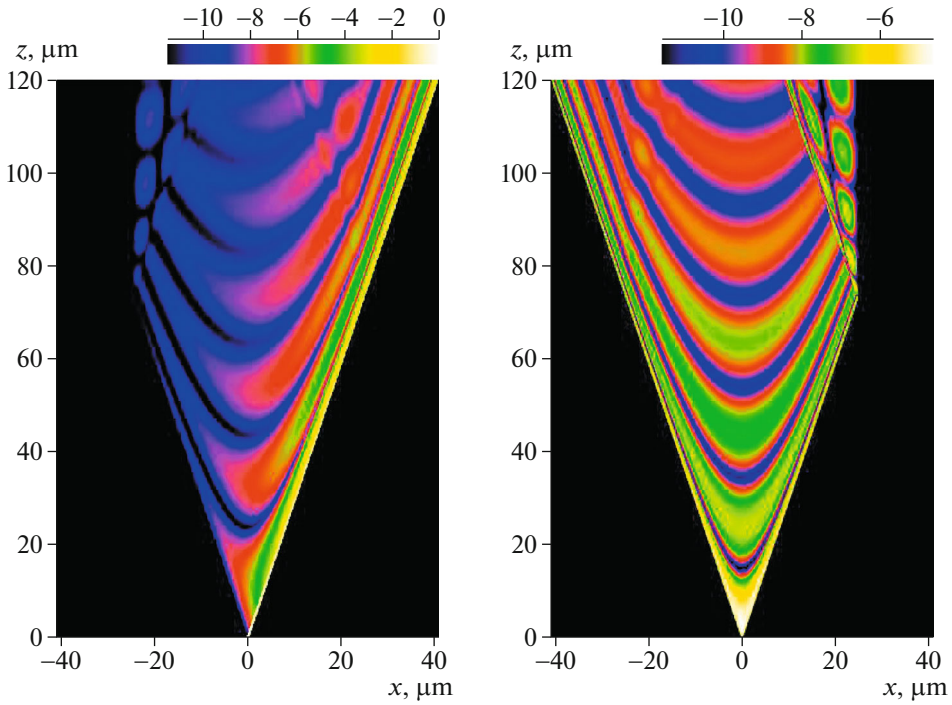

Fig. 2. Distribution of the natural logarithm of relative intensity for the transmitted beam $\ln(I_T/I_0)$ (on the left) and for the reflected beam $\ln(I_R/I_0)$ (on the right) inside the Borrmann fan. A narrow beam is incident on the crystal end face. A version of section topogram in the Laue geometry. The silicon crystal sizes are 50 μm along the *X* axis and 120 μm along the *Z* axis, reflection 220, photon energy $E = 10$ keV.

I_{ma}/I_0; $I_{mi} = MI_{ma}$. All values smaller than I_{mi} were replaced with I_{mi}. The factor M was chosen empirically to obtain the best contrast. This must be done, because $\ln(0) = -\infty$. If a too small M value is chosen, the contrast of maximum values will be very weak; in the case of too large M, the contrast of small values will disappear. The color scale above the image shows the $\ln(I_n/I_0)$ values, where $n = T, R$.

Note that at small z values the image in reflected beam shows the well-known symmetric Kato interference fringes [5] of section topography, and the crystal boundary manifests itself in no way. Beginning with $z = 73$ μm, the intensity on the right side of Fig. 2 is limited by the crystal width, and on the left it becomes constant along the lines parallel to the vector $\mathbf{k}_h$. The pattern for the transmitted beam is asymmetric, and limitation by the crystal width occurs on the left.

The incident narrow beam remains fairly intense throughout the entire crystal length, with intensity significantly exceeding the diffracted radiation intensity. One can draw the following conclusion: the diffraction of a narrow beam is not quite dynamic, because the diffracted wave weakly affects the incident wave (despite the fact that interference occurs). In the case of diffraction of a wide beam the pattern is radically different. This fact has been discussed poorly, although it is clearly demonstrated in the analytical theory. The maximum relative reflection I_R/I_0 is reached very rapidly (i.e., at small z values); it is about 0.01.

Second case. The crystal has a width $W_c = 30$ μm and a length $L_c = 250$ μm. The incident beam has a relatively large width ($S = 100$ μm), and its center is shifted to the left by −64.2 μm. As a result, the incident beam illuminates only the left lateral surface of the crystal, and this situation corresponds to the Bragg diffraction. It is known from the analytical theory for plane waves that total external reflection occurs in this case under the condition $|\alpha - 2\mathrm{Re}(\chi_0)| < |\mathrm{Re}(\chi_h)|$. Therefore, the angular deviation was chosen from the condition $\alpha = 2\mathrm{Re}(\chi_0)$; specifically, $\Delta\theta = 16.088 \times 10^{-6}$ μrad.

The convergence scheme was chosen so as to obtain the final result not only on the crystal end face but also in the region formed during the wave reflection from a crystal lateral face. A crystal of length L can reflect a beam by the width $W = L\tan(\theta_B)$. At $L = 250$ μm we have $W = 85.3$ μm. For this reason the size $2W + W_c = 200.6$ μm is shown. The logarithmic scale (i.e., the value $\ln(I_n/I_0)$, where $n = T, R$) was used again to show the weak wave field inside the crystal.

The calculation results are presented in Fig. 3. The transmitted-beam intensity map demonstrates that the width of the incident beam exceeds the value necessary for illuminating the entire crystal lateral face. The left part of the beam just passes through the computa-

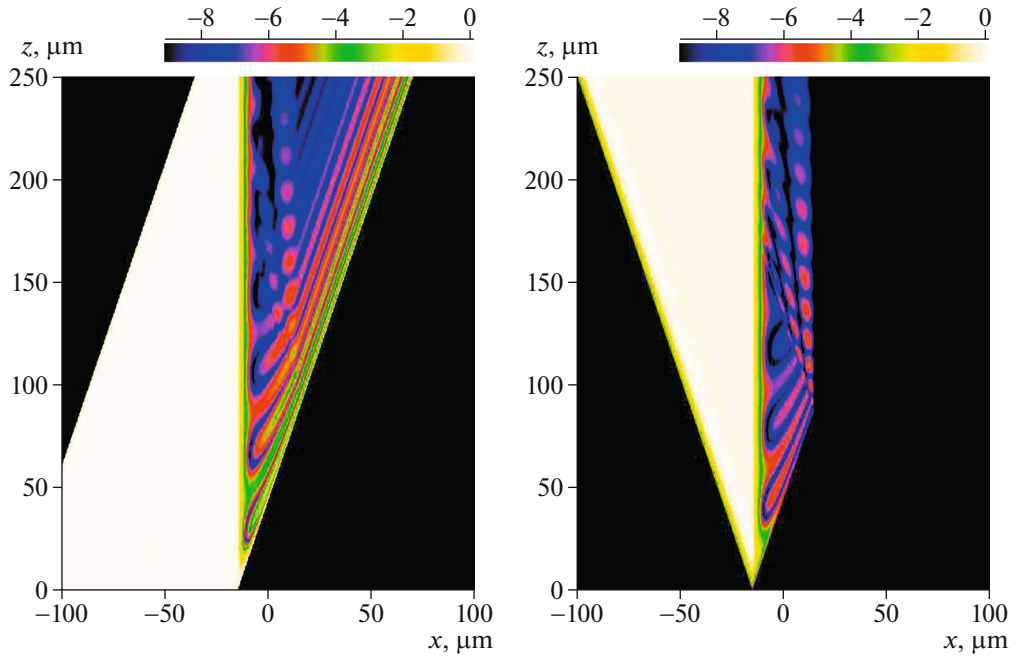

Fig. 3. Distribution of the natural logarithm of relative intensity for the transmitted beam $\ln(I_T/I_0)$ (on the left) and for the reflected beam $\ln(I_R/I_0)$ (on the right). A wide beam is incident on a crystal lateral face. Total external reflection in the Bragg geometry. The silicon crystal sizes are 30 μm along the X axis and 250 μm along the Z axis, reflection 220, photon energy $E = 10$ keV.

tional box without any changes, whereas the part of the beam that enters the crystal differently changes in it at small and large z values. The incident beam reaches the right crystal boundary at $z = 88$ μm. Up to this point the crystal reflects as a thick one, after which the presence of its right boundary corrects the nature of changes in the relative intensity.

These changes are most pronounced in the reflected beam. Correspondingly, the reflected beam in vacuum changes on a double distance of 176 μm. Note the following two features, which are insufficiently clearly presented on the logarithmic scale. The first is that the total reflection occurs not immediately. At very small z values the reflection is weak, and it increases gradually. In other words, the total reflection occurs with a delay. This situation can be compared with the Goos–Hänchen effect, which was discussed for neutrons in [23]; however, it occurs for radiation of any nature upon reflection. In addition, the transition to total reflection is accompanied by oscillations, and the relative intensity of reflected beam in maxima may even exceed unity.

The second feature is that at the same place the transmitted beam penetrates the crystal to a very large depth. In the version considered above it emerges from the crystal with only half intensity lost (partially because of the absorption). The main calculation result in this case is the distribution of relative intensity in the output plane, i.e., on the X axis at the maximum value of the z coordinate. This distribution for the reflected beam is shown in more detail in Fig. 4. The behavior of the curve changes at $x = x_0 = -40$ μm. This point corresponds to the emergence from the crystal for the ray reflected for the first time from its right edge simultaneously with the ray reflected from the left edge.

Note that the analytical formula for this curve was published for the first time as long ago as in 1971 [17]. In the designations of this paper, in the initial stage, when the right crystal boundary does not affect the result, it has the form

$$I_R(x)/I_0 = \left|\frac{B}{2}\int_0^x dx_1 G_0(x_1)\exp(-\mu x_1)\right|^2, \qquad (6)$$
$$B = \frac{K\chi_h}{2\sin\theta_B}, \quad \mu = \frac{K\,\mathrm{Im}(\chi_0)}{2\sin\theta_B},$$

where

$$G_0(x) = J_0(Bx) + J_2(Bx). \qquad (7)$$

Hereinafter, $J_n(z)$ is a Bessel function of the nth order.

The result of the calculation based on this formula is in complete agreement with the curve in Fig. 4, if the coordinate is counted from the left edge, corresponding to the crystal illumination onset. Coincidence occurs at $x < x_0 = 60.3$ μm. After this point, as was shown in [17], the function $G_0(x)$ should be supplemented with the following additional function:

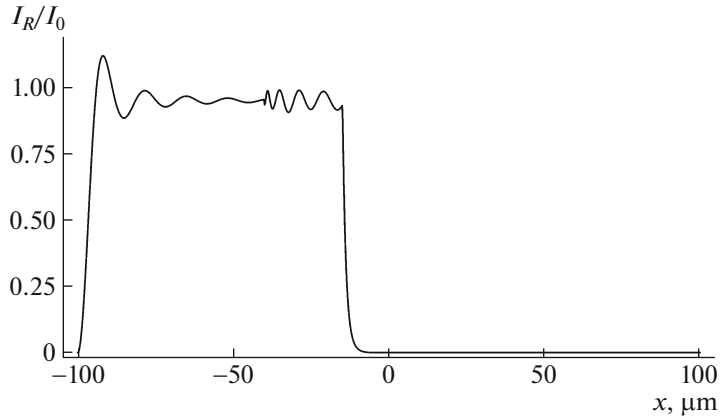

Fig. 4. Detailed distribution of the relative intensity for the reflected beam, presented on the top horizontal line in Fig. 3 (on the right).

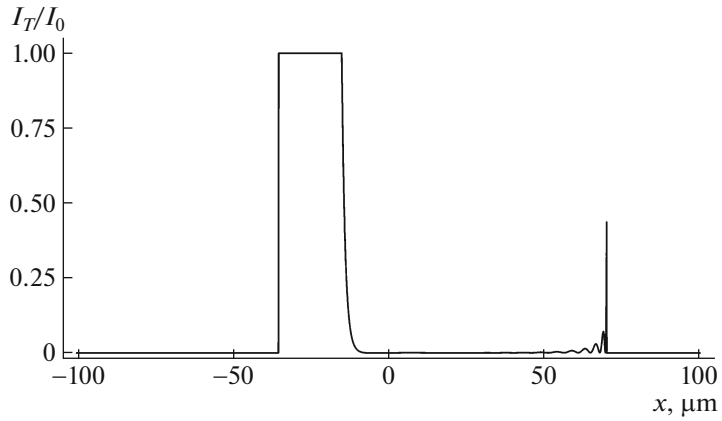

Fig. 5. Detailed distribution of relative intensity for the transmitted beam, presented on the top horizontal line in Fig. 3 (on the left).

$$G_1(x) = -[J_0(B\eta) + 2\xi J_2(B\eta) + \xi^2 J_4(B\eta)],$$
$$\xi = \frac{x - x_0}{x + x_0}, \quad \eta = (x^2 - x_0^2)^{1/2}. \tag{8}$$

By definition this function is zero at imaginary values of the parameter η, i.e., at $x < x_0$. The coordinate x_0, as was noted above, corresponds to the position of the ray reflected for the first time from right crystal face.

The distribution for the transmitted beam is shown in more detail in Fig. 5. Here, we are interested in only the narrow peak on the right side of the curve. This is the part of the beam right edge that was very weakly reflected by the crystal. It shows how a very narrow beam is reflected. The total reflection effect is absent for it. The diffracted radiation intensity is as weak as in the case of Laue diffraction. The calculation scheme under consideration may well contain parts of the beam that change in no way when passing by crystalline regions. This is also specially demonstrated in the plot. Here, an interesting detail is that the left and right edges are limited by the slit and crystal, respectively. One can see how rapidly (but not instantaneously) the radiation disappears in the crystal under total reflection conditions.

CONCLUSIONS

The new scheme for numerical simulation of the effect of coherent dynamic diffraction of synchrotron radiation in crystals of arbitrary shape and structure proved its efficiency. In this scheme the boundary conditions for solving the Takagi–Taupin equations are not linked to the crystal boundaries. The latter are determined in terms of functions of coordinate z. This scheme makes it possible to solve many various problems concerning the simulation of diffraction in crystals of complex shape.

The results of numerical solution of the equations within the same scheme are presented for two examples: the diffraction of a narrow beam in the Laue geometry and the diffraction of a wide beam in the

Bragg geometry. The calculation results completely coincide with the previous analytical solutions, but the results of numerical solutions are more informative: they yield, in particular, a detailed intensity distribution through the entire crystal volume.

FUNDING

This study was supported by the Russian Foundation for Basic Research, project no. 19-29-12043mk, in the part of developing the computer program, and by the Ministry of Science and Higher Education of the Russian Federation (grant no. 075-15-2021-1362) in the part of the computer experiment.

CONFLICT OF INTEREST

The author declares that he has no conflicts of interest.

REFERENCES

1. A. Authier, *Dynamical Theory of X-ray Diffraction* (Oxford Univ. Press, 2005).
2. Z. G. Pinsker, *Dynamic Scattering of X-rays in Crystals* (Springer, 1978).
3. B. K. Vainshtein, V. M. Fridkin, V. L. Indenbom, et al., *Modern Crystallography,* in 4 vols. (Nauka, Moscow, 1979).
4. N. Kato and A. R. Lang, Acta Crystallogr. **12**, 787 (1959). https://doi.org/10.1107/S0365110X61001625
5. N. Kato, Acta Crystallogr. **14**, 627 (1961). https://doi.org/10.1107/S0365110X61001947
6. S. Takagi, Acta Crystallogr. **15**, 1611 (1962). https://doi.org/10.1107/S0365110X62003473
7. D. Taupin, Acta Crystallogr. **23**, 25 (1967). https://doi.org/10.1107/S0365110X67002063
8. J. Gronkowski, Phys. Rep. **206**, 1 (1991). https://doi.org/10.1016/0370-1573(91)90086-2
9. E. V. Suvorov and I. A. Smirnova, Phys.-Uspekhi **58**, 833 (2015). https://doi.org/10.3367/UFNe.0185.201509a.0897
10. I. L. Shul'pina, E. V. Suvorov, I. A. Smirnova, et al., Tech. Phys. **92**, 1450 (2022).
11. V. G. Kohn and I. A. Smirnova, Acta Crystallogr. A **76**, 421 (2020). https://doi.org/10.1107/S2053273320003794
12. V. G. Kohn and I. A. Smirnova, Crystallogr. Rep. **65**, 515 (2020). https://doi.org/10.1134/S1063774520040124
13. A. Authier, C. Malgrange, and M. Tournarie, Acta Crystallogr. A **24**, 126 (1968). https://doi.org/10.1107/S0567739468000161
14. A. G. Shabalin, O. M. Yefanov, V. L. Nosik, et al., Phys. Rev. B **96**, 064111 (2017). https://doi.org/10.1103/PhysRevB.96.064111
15. V. Punegov and S. Kolosov, J. Appl. Crystallogr. **55**, 320 (2022). https://doi.org/10.1107/S1600576722001686
16. M. Carlsen and H. Simons, Acta Crystallogr. A **78**, 395 (2022). https://doi.org/10.1107/S2053273322004934
17. A. M. Afanas'ev and V. G. Kohn, Acta Crystallogr. A **27**, 491 (1971). https://doi.org/10.1107/S0567739471000962
18. V. G. Kohn and T. S. Argunova, Phys. Status Solidi B **259**, 2100651 (2022). https://doi.org/10.1002/pssb.202100651
19. V. G. Kohn and I. A. Smirnova, Phys. Status Solidi B **257**, 1900441 (2020). https://doi.org/10.1002/pssb.201900441
20. V. G. Kohn and I. A. Smirnova, Crystallogr. Rep. **65**, 508 (2020). https://doi.org/10.1134/S1063774520040112
21. V. G. Kohn. http://xray-optics.ucoz.ru/XR/xrwp.htm
22. V. G. Kohn. http://kohnvict.ucoz.ru/jsp/3-difpar.htm
23. V. A. Bushuev and A. I. Frank, Phys.-Uspekhi **61**, 952 (2018). https://doi.org/10.3367/UFNe.2017.11.038235

Translated by Yu. Sin'kov